CSIRO PUBLISHING

Exploration Geophysics
http://dx.doi.org/10.1071/EG15127

Gas hydrate saturation and distribution in the Kumano Forearc Basin of the Nankai Trough

Jihui Jia[1] Takeshi Tsuji[2,4] Toshifumi Matsuoka[3]

[1]Department of Urban Management, Kyoto University, C1-1-118 Kyotodaigaku-Katsura, Nishikyo-ku, Kyoto 615-8540, Japan.
[2]International Institute for Carbon-Neutral Energy Research (I2CNER) and Faculty of Engineering, Kyushu University, 744 Motooka Nishi-ku, Fukuoka 819-0395, Japan.
[3]Fukada Geological Institute, 2-13-12 Honkomagome Bunkyo-ku, Tokyo 133-0021, Japan.
[4]Corresponding author. Email: tsuji@i2cner.kyushu-u.ac.jp

Abstract. The Kumano Forearc Basin is located to the south-east of the Kii Peninsula, Japan, overlying the accretionary prism in the Nankai Trough. The presence of gas hydrate in submarine sediments of the forearc basin has resulted in the widespread occurrence of bottom simulating reflectors (BSRs) on seismic profiles, and has caused distinct anomalies in logging data in the region. We estimated the *in situ* gas hydrate saturation from logging data by using three methods: effective rock physics models, Archie's equation, and empirical relationships between acoustic impedance (AI) and water-filled porosity. The results derived from rock physics models demonstrate that gas hydrates are attached to the grain surfaces of the rock matrix and are not floating in pore space. By applying the empirical relationships to the AI distribution derived from model-based AI inversion of the three-dimensional (3D) seismic data, we mapped the spatial distribution of hydrate saturation within the Kumano Basin and characterised locally concentrated gas hydrates. Based on the results, we propose two different mechanisms of free gas supply to explain the process of gas hydrate formation in the basin: (1) migration along inclined strata that dip landwards, and (2) migration through the faults or cracks generated by intensive tectonic movements of the accretionary prism. The dipping strata with relatively low AI in the forearc basin could indicate the presence of hydrate formation due to gas migration along the dipping strata. However, high hydrate concentration is observed at fault zones with high pore pressures, thus the second mechanism likely plays an important role in the genesis of gas hydrates in the Kumano Basin. Therefore, the tectonic activities in the accretionary wedge significantly influence the hydrate saturation and distribution in the Kumano Forearc Basin.

Key words: basin analysis, hydrates, inversion, rock physics, saturation, seismic reflection.

Received 22 December 2015, accepted 24 December 2015, published online 12 February 2016

Originally submitted to SEGJ 28 September 2015, accepted 14 December 2015

Introduction

Gas hydrates are ice-like crystalline solids that consist of both water and gas molecules. In a gas hydrate, water molecules form a rigid lattice of cages within which natural gas (mainly methane) is commonly held as a 'guest' (Kvenvolden, 1993; Sloan and Koh, 2007). The occurrence of gas hydrates in nature is constrained by a relatively narrow range of high pressure and low temperature, and it depends on the existence of free gas in the pore space. The gas hydrates that occur in marine sediments of active and passive margins account for more than 90% of the total amount of gas hydrates, and the rest is found in the permafrost of plateaus and arctic regions (Waite et al., 2009).

In the Nankai subduction zone, where the Philippine Sea plate is subducting beneath the Japanese islands (Figure 1*a*), bottom simulating reflectors (BSRs) are widely observed on the seismic profiles (Ashi et al., 2002; Baba and Yamada, 2004; Matsumoto et al., 2004; Uchida et al., 2004). A BSR is a strong reflection with reverse polarity when compared to seafloor reflection, and is considered to be a reflection from the base of the gas hydrate stability zone. Because of the presence of gas hydrates in the sediments, the physico-chemical properties of the sediments are significantly affected. The gas hydrate-bearing sediments have a distinctly high sonic (P-wave) velocity and resistivity when compared with water-saturated sediments (Lee and Collett, 2001; Waseda and Uchida, 2004; Malinverno et al., 2008; Collett and Lee, 2012). These anomalies have been observed in the borehole data obtained within the Kumano Forearc Basin located to the south-east of the Kii Peninsula, overlying the Nankai accretionary prism (Inamori and Hato, 2004; Matsumoto et al., 2004; Waseda and Uchida, 2004; Fujii et al., 2008; Expedition 314 Scientists, 2009*a*, Saito et al., 2010; Strasser et al., 2014; Miyakawa et al., 2014). The total amount of methane contained in gas hydrate-bearing sediments in the south-eastern Nankai Trough has been estimated to be 40 trillion cubic feet (Fujii et al., 2008).

Studies of gas hydrates are of interest because it is thought that large amounts of methane may be recovered from gas hydrates and used as a future energy resource. Alternatively, the decomposition of gas hydrates occurring in marine sediments could lead to geologic hazards such as submarine slumps and induced earthquakes (Kvenvolden, 1993; Sloan and Koh, 2007; Waite et al., 2009). Here, we have focused on the methane hydrates deposited in the Kumano Forearc Basin (He et al., 2006; Tsuji et al., 2009).

There have been numerous studies on hydrate-bearing sediments in the Kumano Basin: Saito et al. (2010) identified

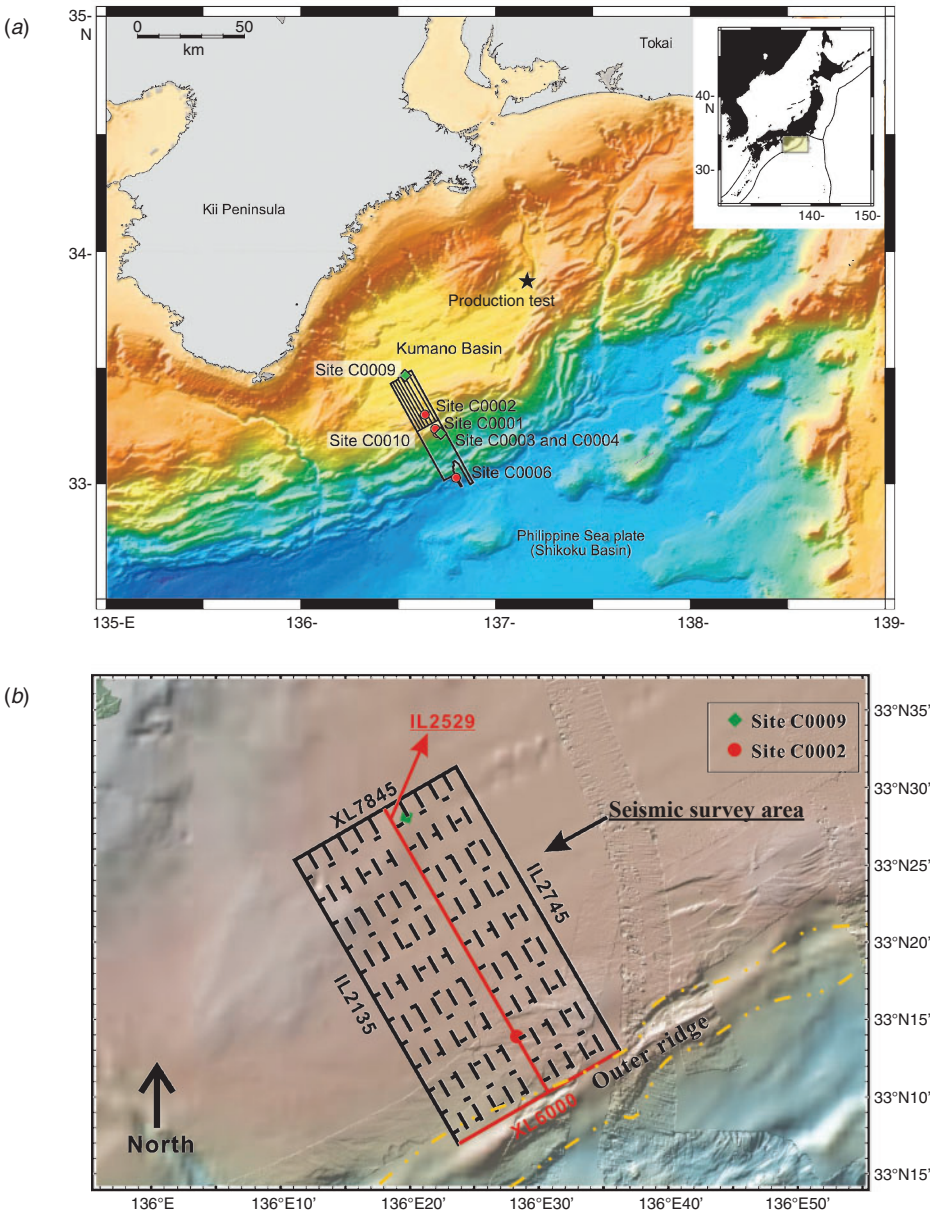

Fig. 1. (*a*) 3D seismic survey area and locations of boreholes in the Nankai Trough (Expedition 319 Scientists, 2010). (*b*) The study area in the Kumano Forearc Basin (crosslines 6000–7845 and inlines 2135–2745). The two red lines represent inline 2529 displayed in Figure 2*a* and crossline 6000 displayed in Figure 2*b*. The south-east edge of this study area corresponds to the outer ridge.

gas hydrate-bearing zones using logging-while-drilling data; Tsuji et al. (2011*a*) estimated seismic velocity and the stress state around the gas-bearing zone using walk-around vertical seismic profiling data; Doan et al. (2011) quantified the distribution of free gas in the landward side of the basin using logging data, and discovered an abundance of wood fragments and lignite in the deeper part of the drilling site C0009; Toki et al. (2012) addressed the formation and accumulation of methane in the pore water extracted from sediments at a drilling site in the Kumano Basin (Site C0002) and from sites on the slope on the seaward side of the Kumano Basin; and Miyakawa et al. (2014) estimated the degree of gas hydrate saturation at Site C0002 in the Kumano Basin using core samples and logging data. In 2013, the first offshore production test of gas hydrates was conducted in the north-eastern part of the Kumano Basin (the black star in Figure 1*a*; Boswell, 2013).

The aim of this study was to better understand the micro-scale physical form and large-scale spatial distribution of gas hydrates in the Kumano Forearc Basin; more specifically, to find where gas hydrates occur in the subsurface sediments both microscopically and macroscopically. We applied rock physics approaches (Dvorkin and Nur, 1996; Helgerud et al., 1999; Helgerud, 2001) to relate the sonic velocity to gas hydrate saturation, and obtained an appropriate model of gas hydrates occurrence. Subsequently, we estimated the spatial distribution of the hydrate saturation along the BSR in the Kumano Basin using three-dimensional (3D) seismic data (i.e. acoustic impedance distribution), which was based on the relationship between acoustic impedance and water-filled porosity (Lu and McMechan, 2002; Wang et al., 2011). Finally, we postulated probable explanations regarding the genesis of gas hydrates in the Kumano Basin.

Data

Seismic data

In 2006, a 3D seismic reflection survey covering an area of ~600 km^2 in the Nankai Trough was conducted. The seismic data also cover the southern part of the Kumano Forearc Basin (Figure 1*b*). As sound source, two arrays were deployed, each with 28 air guns, fired alternately at 37.5 m shot intervals. The survey used four receiver cables spaced 150 m apart, each 4500 m long with 360 receiver groups at a 12.5 m spacing (Moore et al., 2009). Seismic processing mainly included true amplitude recovery with spherical divergence corrections and exponential gain, F-K filtering to remove linear noise, and Kirchhoff anisotropic pre-stack time migration. The orientation of the inlines was south-east–north-west (perpendicular to the convergent margin) with a spacing of 18.75 m, and the spacing of crosslines (which were oriented south-west–north-east) was 12.5 m. The seismic resolution was ~5–7 m for the near-surface sediments (Moore et al., 2009). The base of the gas hydrates is identified in the seismic data as BSRs (Figure 2), which are widely distributed within the Kumano Basin sediments (Ashi et al., 2002; Baba and Yamada, 2004; Tsuji et al., 2009). In this paper, we analysed the 3D seismic data from crosslines 6000–7845 and inlines 2135–2745, which correspond to the southern part of the Kumano Basin (Figure 1*b*).

On the seismic profile (inline 2529) intersecting the drilling site C0002 (Figure 2*a*), a remarkable BSR (indicated by small black arrows) was observed at around 3.1 s in two-way traveltime, corresponding to 400 m below seafloor (mbsf) in

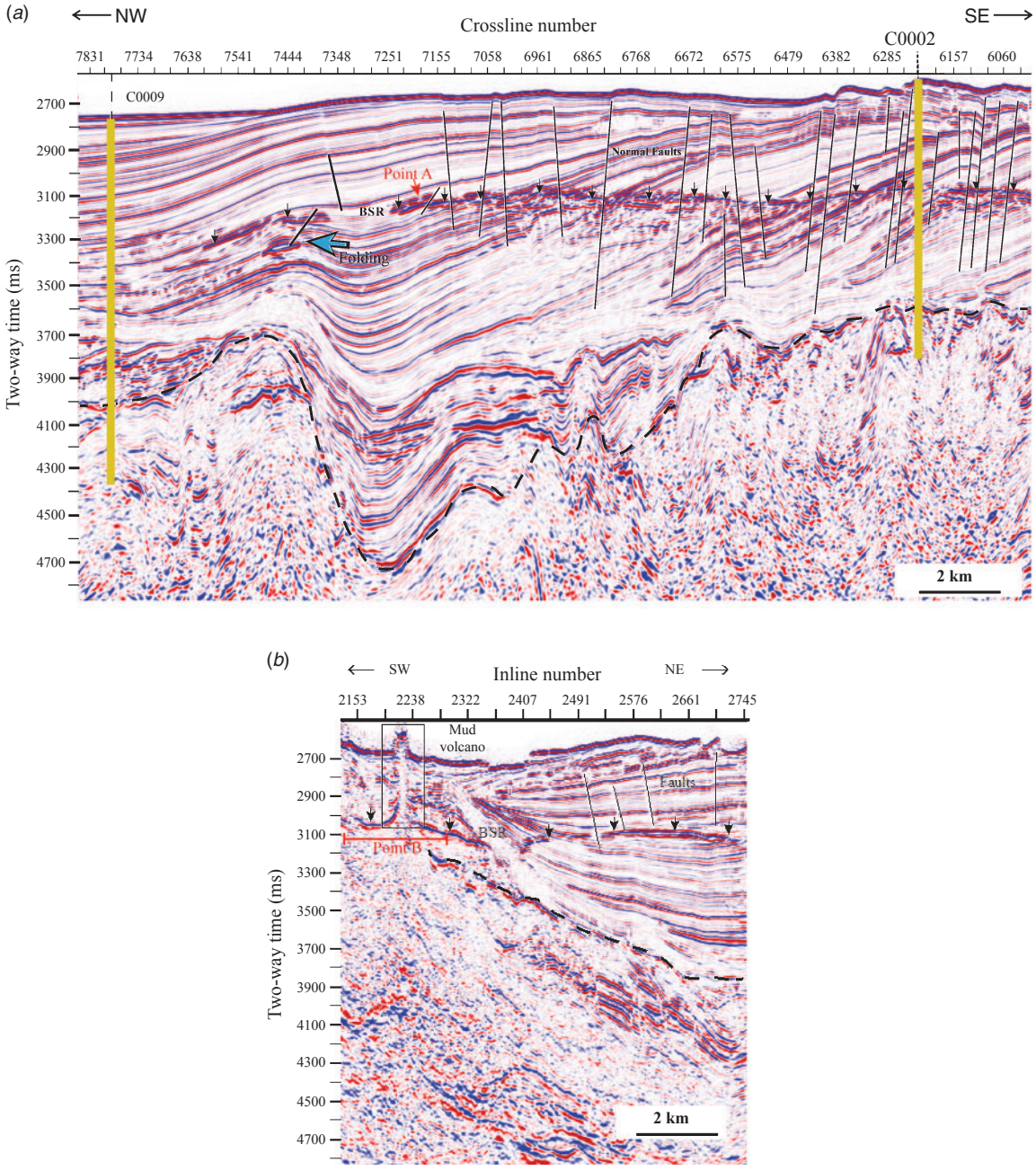

Fig. 2. (*a*) Seismic section (inline 2529) extracted from 3D seismic data that intersects Site C0002. The strong reflection at ~3100 ms indicates the BSR (black arrows). The two thick yellow lines represent the locations of the two drilling sites. The dash line is the interface between sediments and the underlying accretionary prism. The solid lines symbolise the normal faults occurring in the area. (*b*) Seismic section (crossline 6000) extracted from 3D seismic data showing a mud volcano (black rectangle).

depth at this site. It extends continuously for ~15 km from the outer ridge to landward (Figure 1*b*) (north-west direction) and becomes increasingly deeper and discontinuous, indicating higher temperatures around the outer ridge (Hamamoto et al., 2011; Kinoshita et al., 2011). The interface between the forearc basin sequence and the underlying accretionary prism (dashed line in Figure 2) can be clearly observed on seismic profiles. In the Kumano Basin, the strata of the sediment sequence dipping landward are cut by many normal faults (solid lines in Figure 2). There are no clear reflections in the accretionary prism beneath the Kumano Basin, since the lithology is consolidated and the structures are complicated or steeply dipping (Tsuji et al., 2014*a*).

A seismic profile of crossline 6000 in the Kumano Forearc Basin (Figure 2*b*) exhibits a clear BSR (indicated by small black arrows) as well as a mud volcano (inside rectangular frame). It has been reported that the areas around mud volcanoes in many places have abnormal pressure-temperature conditions that facilitate the formation of gas hydrates (Kvenvolden, 1993; Sloan and Koh, 2007). This seismic profile further shows that the mud volcano penetrates through the BSR, which is shallower close to the mud volcano, indicating a local high heat flow anomaly due to upward fluid flow from deeper sediments (Milkov, 2000; Hamamoto et al., 2011).

Logging and core data

The Integrated Ocean Drilling Program has drilled many boreholes at a dozen sites within the 3D seismic survey area off Kumano (Saffer et al., 2009; Expedition 314 Scientists, 2009*a*; Expedition 319 Scientists, 2010; Strasser et al., 2014). The green squares and red dots in Figure 1*a* represent drilling sites from expedition 319 and expeditions 314/315/338, respectively (Expedition 319 Scientists, 2010; Expedition 314 Scientists, 2009*a*; Strasser et al., 2014). The drilling sites are distributed in the forearc basin (C0002 and C0009), in the accretionary wedge on the seaward side of outer ridge (C0001, C0003, C0004, C0010) and within the frontal thrust zone (C0006). Various kinds of logging data and core samples were acquired at these sites.

Site C0002 is of most importance to this study, because gas hydrates were identified by both logging data and interstitial water data extracted from core samples. This site is located near the seaward (south-east) edge of the Kumano Basin close to the outer ridge (Figure 1*b*). The logging data used here is from seafloor to 951 mbsf including neutron porosity, density, sonic velocity and near-bit resistivity logs of high quality (Figure 3*a*). Gas hydrates were inferred from 218.1 to 400.4 mbsf due to abnormally high P-wave velocities and high resistivities in the logging data (Expedition 314 Scientists, 2009*a*). The gas hydrates could elevate P-wave velocities by stiffening the host sediment, and they also enhance resistivity because gas hydrates are non-conductive materials (Waite et al., 2009). In Figure 3*a* the values of P-wave velocity, acoustic impedance and resistivity decrease sharply at the depth corresponding to the BSR (~400 mbsf). A gas-bearing zone can be identified by low densities and velocities from 481.6–547.1 mbsf. The porosity from the neutron log is influenced by both water and hydrates in the sediments, because it detects only hydrogen in the formation. In addition, the variations of mineral composition with depth were obtained by X-ray diffraction (XRD) analysis of the core samples (Strasser et al., 2014). The mean values and the standard deviations of quartz proportion are $28.5 \pm 5.8\%$, $28.8 \pm 5.1\%$ and $23.4 \pm 5.7\%$ for the gas hydrate zone, the free gas zone and the sedimentary section below 580 mbsf, respectively.

Site C0009 is on the landward side of the Kumano Forearc Basin, around 20 km north-west of Site C0002 (Figure 1). At this drilling site, wireline downhole logging was carried out (Expedition 319 Scientists, 2010). The casing was set down to 713 mbsf, and logging data were recorded from 713.84 mbsf to 1554.6 mbsf. The porosity curve shown in Figure 3*b* was calculated from density data rather than neutron porosity data because the former was of higher quality than the latter in this borehole (Expedition 319 Scientists, 2010). Based on the analysis of cuttings and monitoring of mud gas, it was identified that the green shaded area in Figure 3*b* (791–1285 mbsf) was a zone of concentrated free gas relative to the units above and below. The bottom of this interval (dark green area in Figure 3*b*) was characterised by abundant wood lignite fragments with very high total organic carbon (TOC) content, ranging from 1.5 to 8.7 wt% (Expedition 319 Scientists, 2010). The abnormal low velocity and density (Figure 3*b*) are attributed to the gas enrichment in this unit.

Methods

In investigating the distribution and characteristics of the gas hydrates occurring in the Kumano Basin sediments, we estimated the spatial distribution of the saturation of hydrates. First, we used the following three methods to estimate the hydrate saturation in the borehole at Site C0002: (1) a rock physics model for P-wave velocity data, (2) Archie's equation for resistivity data, and (3) an empirical relationship between acoustic impedance and water-filled porosity. In this study, we considered the result from Archie's equation as a reference because a previous study has derived hydrate saturation using this approach (Miyakawa et al., 2014). By comparing these estimates, we can infer the appropriate microscopic rock physics model for hydrate-bearing sediments, and validate the feasibility of method (3). Subsequently, the logging data from both Sites C0002 and C0009 were employed in the calibration of synthetic seismograms (i.e. fitting the synthetic traces to real traces) in the acoustic impedance inversion. Then we used the relationship of method (3) to assess the spatial distribution of hydrates in the Kumano Basin.

Saturation estimation from P-wave velocity based on rock physics models

We used a first-principle-based effective-medium model to predict the amount of hydrates in sediments from sonic data in Site C0002. The model used here should take into account the effective pressure, porosity and mineralogy of the sediment, and is applicable to unconsolidated, high porosity, ocean bottom sediments bearing gas hydrates (Helgerud et al., 1999; Ecker et al., 2000). The dependence of elastic moduli, and hence seismic velocity, on the location of precipitated hydrates within pore space causes ambiguity when trying to infer hydrate saturations from measured seismic velocities.

We considered two cases for hydrate distribution in pores: (a) a pore-filling model, in which hydrates are floating in the pore fluid and so modify the pore fluid elastic properties without affecting the frame; and (b) a matrix-supporting model, in which hydrates become a component of the solid phase, thereby modifying the elasticity of the frame. Each of these models generates a relationship between P-wave velocity and gas hydrate saturation.

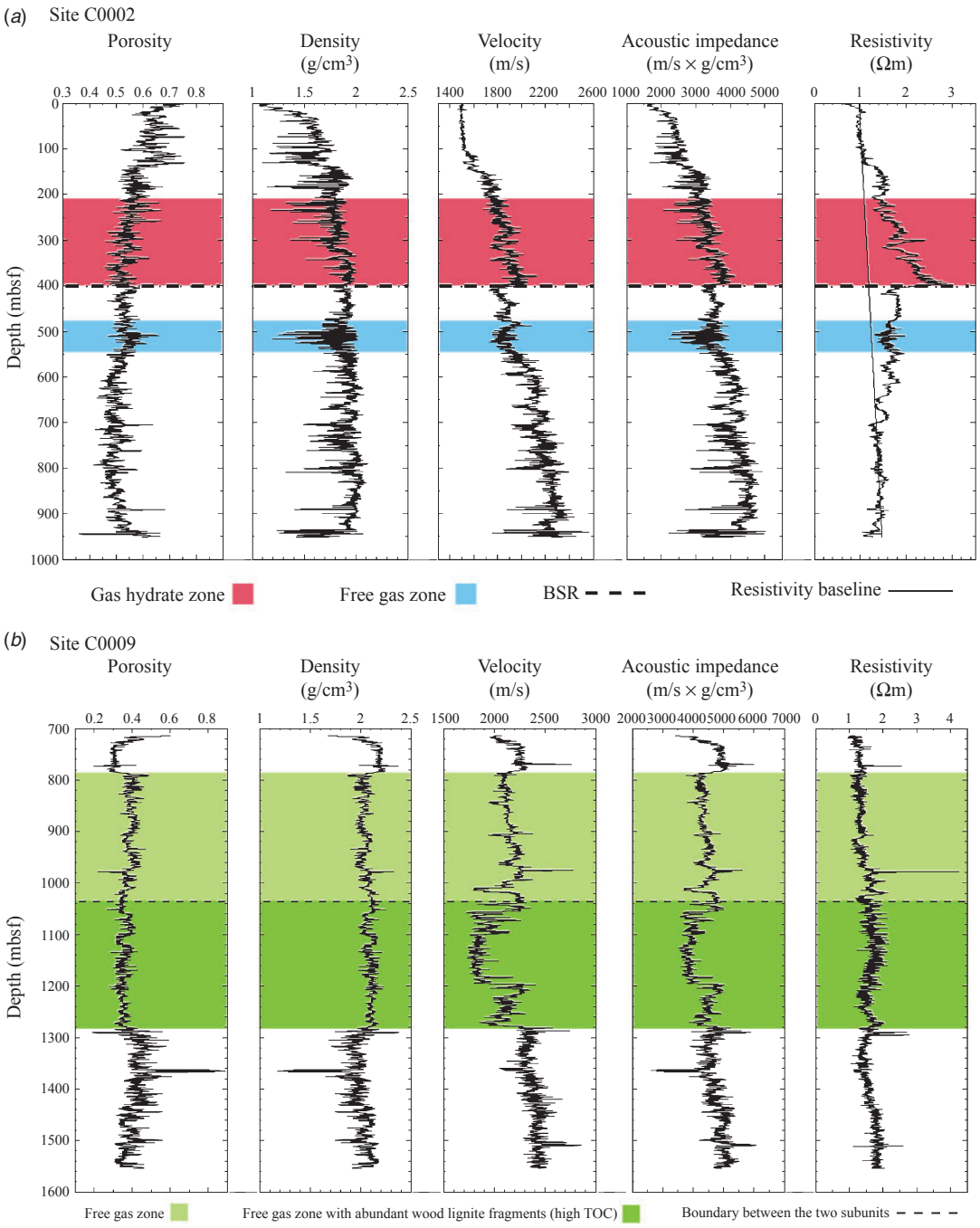

Fig. 3. Logging data obtained at (*a*) Site C0002 and (*b*) Site C0009. The gas hydrate zone and free gas zone identified at Site C0002 are marked by red and blue colouring, respectively. The free gas zone found at Site C0009 is marked by green colouring.

(a) Pore-filling model

In the common case of mixed mineralogy, the effective elastic constants (bulk modulus K_m and shear modulus G_m) of the solid phase are calculated from those of individual mineral constituents using Hill's average formula:

$$M = \frac{1}{2}\left[\sum_{i=1}^{m} f_i M_i + \left(\sum_{i=1}^{m} f_i / M_i\right)^{-1}\right] \quad (1)$$

where M_i represents the elastic modulus of the i-th constituent, f_i is the volumetric fraction of i-th constituent in the solid phase and m is the number of mineral constituents. The relative abundances of individual minerals (clay, quartz, feldspar and calcite) were determined by XRD analysis of the recovered core samples (Expedition 315 Scientists, 2009; Strasser et al., 2014). We used the averaged abundances of these minerals within the gas hydrate zone (Table 1). The solid phase density was calculated as the volumetric average of the individual minerals' densities (Mavko et al., 2009).

The bulk (K_{dry}) and shear (G_{dry}) moduli of dry sediments can be expressed using Hashin-Shtrikman bound theory. For $\phi < \phi_C$, we used the lower Hashin-Shtrikman bound (Dvorkin et al., 1999):

$$K_{dry} = \left[\frac{\phi/\phi_C}{K_{HM}+\frac{4}{3}G_{HM}} + \frac{1-\phi/\phi_C}{K+\frac{4}{3}G_{HM}}\right]^{-1} - \frac{4}{3}G_{HM} \quad (2)$$

$$G_{dry} = \left[\frac{\phi/\phi_C}{G_{HM}+Z} + \frac{1-\phi/\phi_C}{G+Z}\right]^{-1} - Z \quad (3)$$

whereas, for $\phi \geq \phi_C$, we used the upper Hashin-Shtrikman bound as proposed by Dvorkin et al. (1999):

$$K_{dry} = \left[\frac{(1-\phi)/(1-\phi_C)}{K_{HM}+\frac{4}{3}G_{HM}} + \frac{(\phi-\phi_C)/(1-\phi_C)}{\frac{4}{3}G_{HM}}\right]^{-1} - \frac{4}{3}G_{HM} \quad (4)$$

$$G_{dry} = \left[\frac{(1-\phi)/(1-\phi_C)}{G_{HM}+Z} + \frac{(\phi-\phi_C)/(1-\phi_C)}{Z}\right]^{-1} - Z \quad (5)$$

$$Z = \frac{G_{HM}}{6}\left(\frac{9K_{HM}+8G_{HM}}{K_{HM}+2G_{HM}}\right) \quad (6)$$

where ϕ is porosity of sediments, ϕ_C is the critical porosity (0.36–0.40 according to Nur et al. (1998) – we used 0.36 in our calculations) and K_{HM} and G_{HM} represent the effective bulk and shear moduli of the dry frame at critical porosity ϕ_C given by Hertz-Mindlin contact theory (Dvorkin et al., 1999):

$$K_{HM} = \left[\frac{q^2(1-\phi_C)^2 G_m^2}{18\pi^2(1-\nu)^2}P\right]^{\frac{1}{3}} \quad (7)$$

$$G_{HM} = \frac{5-4\nu}{5(2-\nu)}\left[\frac{3q^2(1-\phi_C)^2 G_m^2}{2\pi^2(1-\nu)^2}\right]^{\frac{1}{3}} \quad (8)$$

where q is the average number of contacts per grain at ϕ_C, which is between 8 to 9 (Dvorkin et al., 1999). We set the value as 8.5 in our calculations. G_m and ν are the shear modulus and Poisson's ratio of the solid phase, respectively. P is the effective pressure denoting the difference between hydrostatic and lithostatic pressure, and is calculated from Equation 9:

$$P = (\rho_b - \rho_w)gD \quad (9)$$

where ρ_b is the bulk density of the sediment derived from logging data, ρ_w is the water density (Table 2), g is the acceleration due to gravity and D is the depth below the seafloor.

Because the sediment in the pore-filling model is saturated with pore fluid, including seawater and gas hydrates, the bulk modulus K_{sat} can be calculated from the Gassmann equation (Dvorkin et al., 1999) as follows:

$$K_{sat} = K_{dry} + \frac{\left(1-\frac{K_{dry}}{K_m}\right)^2}{\left(\frac{S_h}{K_h}+\frac{1-S_h}{K_w}\right)\times\phi + \frac{1-\phi}{K_m} - \frac{K_{dry}}{K_m^2}} \quad (10)$$

where S_h is the gas hydrate saturation, which is its volumetric fraction in pore space, and K_h is the bulk modulus of the hydrate (Table 2). The saturated shear modulus G_{sat} is the same as that of the dry frame.

Once the elastic moduli are obtained, the P-wave velocity of hydrated sediments V_p can be obtained by the following equation:

$$V_p = \sqrt{\frac{K_{sat}+\frac{4}{3}G_{sat}}{\rho_{sat}}} \quad (11)$$

where ρ_{sat} represents the bulk density of saturated sediments.

(b) Matrix-supporting model

In this model, gas hydrates are considered to be a part of the mineral matrix, reducing the original porosity as follows:

$$\phi_r = \phi S_w = \phi(1-S_h) \quad (12)$$

where ϕ_r represents reduced porosity due to hydrate precipitation, ϕ is the original porosity in the sediments from logging data and S_w is water saturation.

The elastic moduli of the solid phase (Equation 1) are calculated using both gas hydrates and minerals. The steps to calculate the elastic moduli of dry rocks are same as case (a) using Equations 2–9. For the calculation of saturated bulk modulus (Equation 10), the terms involving gas hydrate saturation are removed because it is assumed that only seawater fills the pore space.

Saturation estimation from resistivity based on Archie's equation

Because gas hydrate is effectively an electrical insulator, we are able to identify gas hydrate-bearing sediments by abnormally high resistivity in well logging data. Further, we can quantify the volume of gas hydrates in the sediments using the resistivity. Archie (1942) proposed this interpretation and it has been extensively utilised in prospecting for hydrocarbons and estimating gas hydrate content in marine sediments (Collett and Ladd, 2000; Lu and McMechan, 2002).

Gas hydrate saturation can be expressed as a function of the ratio of the resistivity of the same formation saturated with water (R_0) to the measured resistivity (R_t). This is given by the following equation (Lu and McMechan, 2002):

$$S_h = 1 - \left(\frac{R_0}{R_t}\right)^{\frac{1}{n}} \quad (13)$$

where n is the saturation exponent, which is an empirical parameter. For hydrated clastic sediments, $n = 1.9386$ (Pearson *et al.*, 1983). R_t is the measured resistivity from logging data and R_0 is the resistivity of the formation fully saturated with water, determined by Equation 14:

$$R_0 = 5.2518 \times 10^{-4} Z + 0.9738. \quad (14)$$

This equation represents the baseline of the near-bit resistivity curve shown in Figure 3*a* fitted from well logging

Table 1. Properties of original rock matrix used in effective-medium modelling.

Mineral type	Total clay minerals	Quartz	Feldspar	Calcite
Bulk modulus (GPa)	20.9	36	37.5	76.8
Shear modulus (GPa)	6.85	45	15	32
Density (g/cm^3)	2.58	2.65	2.62	2.71
Relative abundance	0.48	0.28	0.18	0.06

Table 2. Properties of pore water and methane hydrate in effective-medium modelling.

Material	Pore water (brine)	Methane hydrate
Bulk modulus (GPa)	2.5	5.6
Shear modulus (GPa)	–	2.4
Density (g/cm^3)	1.032	0.9

data using the top (0–138 mbsf) and bottom (641.5–950.7 mbsf) of the dataset. Z is the depth below the seafloor in metres.

Saturation estimation from acoustic impedance based on an empirical relationship

First, we estimated water-filled porosity in the sediments by Archie's equation:

$$\phi_w = \left(\alpha \frac{R_w}{R_t}\right)^{\frac{1}{\beta}} \quad (15)$$

where ϕ_w is the water-filled porosity in the sediments, α and β are environment-dependent empirical constants, which we set as $\alpha = 1$ and $\beta = 2.4$ following an IODP report (Expedition 314 Scientists, 2009*b*), and R_w is the resistivity of the pore water, which is mainly a function of the temperature of the seawater and can be calculated from the following formula:

$$R_w = \frac{1}{2.8 + 0.1T} \quad (16)$$

where T is formation temperature determined by using seafloor temperature and the thermal gradient at Site C0002 (Expedition 314 Scientists, 2009*b*; Expedition 315 Scientists, 2009).

Second, we established a relationship between acoustic impedance and water-filled porosity derived from Equation 15. Herein, the logging data from borehole C0002A are divided into three groups as a function of depth: a gas hydrates zone, a free gas zone and a water-saturated zone. Here, we consider only the gas hydrate zone and the water-saturated zone. The relationships between acoustic impedance and water-filled porosity can be represented by polynomials, whose coefficients are found by least-squares fitting to the data and are given in the following equations,

For the gas hydrates zone:

$$\phi_w = -4.9115 \times 10^{-8} I^2 + 2.2961 \times 10^{-4} I + 0.2135 \quad (17)$$

where I represents acoustic impedance. The average difference between the fitting values and those calculated from logging data is 0.019 with standard deviation 0.016.

For the water-saturated zone:

$$\phi_w = 1.1933 \times 10^{-11} I^3 - 8.6929 \times 10^{-8} I^2 + 6.4967 \times 10^{-5} I + 0.7727. \quad (18)$$

The average difference between the fitting values and those calculated from logging data for this interval is 0.017 with standard deviation 0.021. In the cross-plot of water-filled porosity against acoustic impedance (Figure 4*a*), the black line is the curve (Equation 18) fitted to the data points from the water-saturated zones only. In Figure 4*b*, the pink curve is that (Equation 17) fitted to the data points from the gas hydrate-bearing zone. Also shown in Figure 4*b* is the 'background line' of Equation 18. Nearly all the red points are below the background line, indicating that gas hydrates have reduced the original pore space in the sediments.

Finally, we can obtain gas hydrate saturation from the water-filled porosity predicted from acoustic impedance using Equation 17 as follows:

$$S_h = 1 - \left(\frac{R_0 \phi_w^{\beta}}{\alpha R_w}\right)^{\frac{1}{n}}. \quad (19)$$

Spatial distribution of hydrate saturation from 3D seismic data

Well logging data provide only one-dimensional information about hydrate saturation. We use 3D seismic data to extend the well information spatially to study gas hydrate distribution within the entire seismic survey area in the Kumano Forearc Basin. Acoustic impedance can be obtained from post-stack seismic data using seismic inversion, and this represents a kind of pseudo-acoustic impedance log at the location of each seismic trace. Within our study interval above the BSR, the background resistivity of the water-saturated sediment calculated from Equation 14 spans from 1.17 to 1.18 Ωm, and the resistivity of pore water derived from Equation 16 varies from 0.21 to 0.22 Ωm, so we assumed that these parameters do not change along the BSR. Consequently, we were able to estimate the spatial gas hydrate saturation from seismic data using the method described above (i.e. the empirical relationship between acoustic impedance and hydrates saturation).

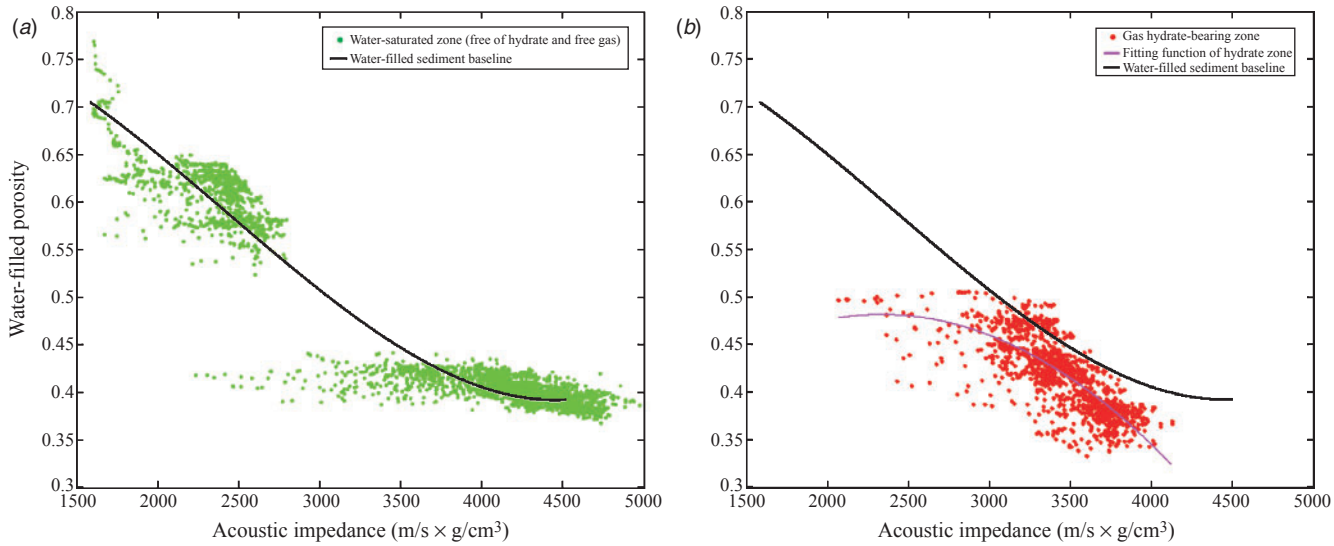

Fig. 4. Cross-plots of water-filled porosity and acoustic impedance at borehole C0002A. (*a*) Green data points are from the water-saturated zone, and the black line is the best-fit polynomical function. (*b*) Red data points are from the gas hydrate-bearing zone, and the pink line is the corresponding best-fit curve. The black curve is the function shown in Figure 4*a*.

Seismic inversion is the process of calculating a subsurface impedance model consistent with corresponding seismic data (Ecker et al., 2000; Lu and McMechan, 2002). The seismic trace is considered as a convolutional result from the reflectivity of the interface of subsurface layers and the wavelet. We used model-based inversion based on the convolutional model:

$$T_i = \sum_j r_j W_{i-j+1} + e_i \tag{20}$$

where T_i is seismic response, r_j is the reflectivity of the earth for a seismic wave expressed as a time series, W_i denotes the seismic wavelet and e_i represents additive measurement noise.

Using this method, the acoustic impedance of subsurface rocks can be obtained from seismic data. However, because of the signal attenuation and geometric spreading during propagation, all of the seismic data become frequency band-limited. Combining seismic data with well log data can solve this problem. Because logging data are *in situ* measurements taken directly at the various depths in the borehole and uninfluenced by attenuation, they can provide an initial model as an input parameter, and guide the performance of the acoustic impedance inversion. The procedure was as follows: (1) set the initial acoustic impedance from the well log data using a specified block size (we initially set it as 2 ms), which represents the thickness of the layer; (2) convolve the blocky model and wavelet to obtain synthetic seismic traces; and (3) use least-squares optimisation to update the impedance to minimise the difference between the real seismic data and the modelled reflectivity traces. Through analysing the misfit between the synthetic traces and seismic traces, as well as modifying the block size repeatedly until the lowest misfit is achieved, the optimum result (i.e. an acoustic impedance volume) is obtained (Swisi, 2009). The correlation coefficient between the waveform synthesised from logging data and the seismic trace at the location of a borehole is as high as 99% for Site C0002 and 98% for Site C0009.

Results and interpretations

Comparison of saturations from different methods

Figure 5 illustrates the estimated hydrate saturations versus depth at Site C0002. The estimated hydrate saturations were filtered by a moving average method with a window size of 61 data points (9.1 m). The red, blue, orange and green lines in Figure 5 represent the results from the pore-filling model, the matrix-supporting model, Archie's equation and the empirical relationship, respectively. All of the curves show similar patterns. Considering the hydrate saturations from rock physics models, we observed that the results from the pore-filling model (red line in Figure 5) indicate notably higher saturations than those calculated using the matrix-supporting model (blue line in Figure 5). The maximum difference between the two results is as large as 0.16 at 385.7 mbsf. The highest saturations occurring at this depth, 0.32 and 0.48, correspond to the matrix-supporting model and pore-filling model, respectively. The result calculated from Archie's equation (orange line in Figure 5) shows a comparable trend to that of the rock physics models except that largest value is at the bottom of the interval. This depth discrepancy would be attributed to the inherent uncertainties from different measurements. As the result from Archie's equation for near-bit resistivity was more stable, we used it for establishing the empirical relationship between acoustic impedance and water-filled porosity (Figure 4). Consequently, the result calculated from the empirical relationship (green line in Figure 5) is almost the same as that from Archie's equation in terms of mean values, which were 0.224 and 0.222, respectively.

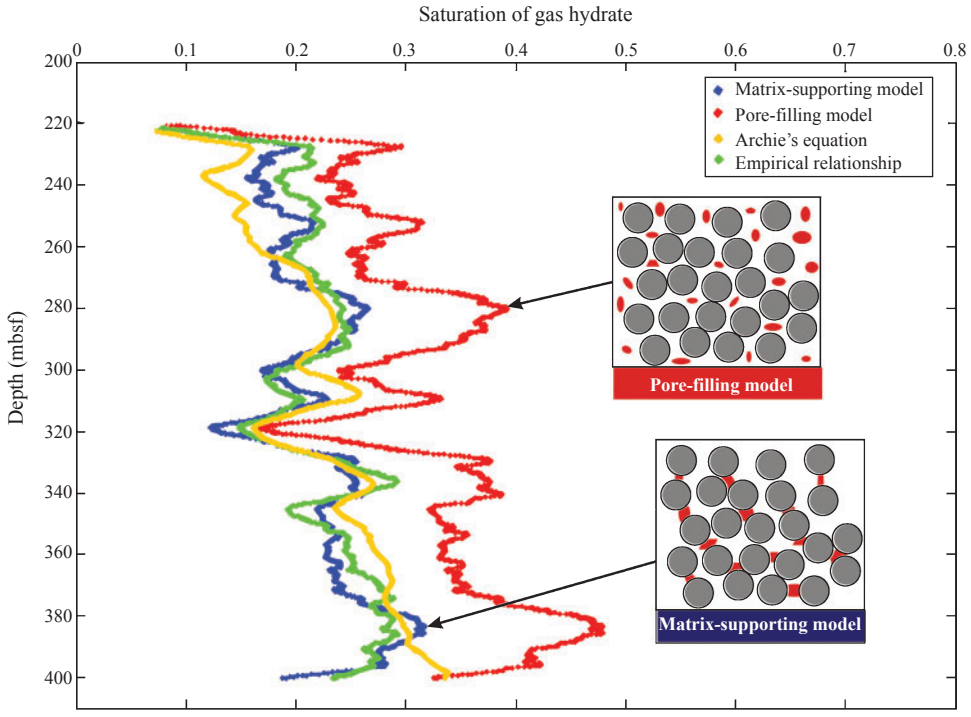

Fig. 5. Gas hydrate saturation estimated from rock physics models (pore-filling model and matrix-supporting model), Archie's equation and an empirical relationship. This figure includes the schematic images of the pore-filling model and matrix-supporting model.

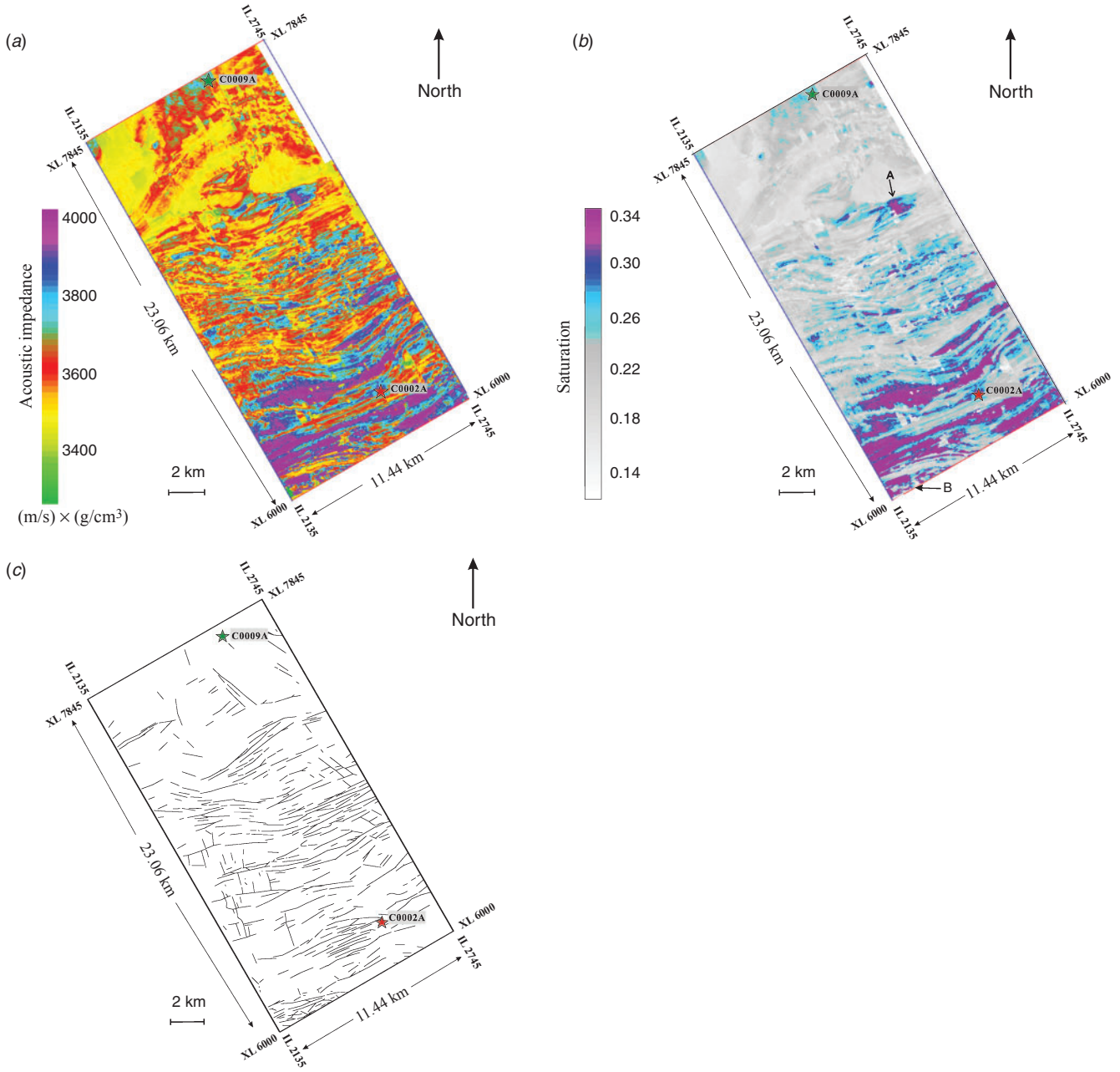

Fig. 6. (*a*) The acoustic impedance along the BSR. The acoustic impedance represents the maximum values extracted from a window with size of 10 ms above the BSR. (*b*) Spatial gas hydrate saturation estimated from panel (*a*). Point A marks a high concentration area on the landward side of the centre of the research area, and point B shows the location of a mud volcano. (*c*) A depth slice at 514 mbsf showing the distribution of normal faults within the Kumano Forearc Basin (modified from Moore et al., 2013).

All of these saturations, estimated using different methods, increase with depth in a similar way, although there are several local minima around 302.5 mbsf, 318.6 mbsf and 344.1 mbsf, indicating relatively low concentration of gas hydrates in the sediments. The mean values from the Archie's equation model ($S_h = 0.222$), the matrix-supporting model ($S_h = 0.217$) and the acoustic impedance model ($S_h = 0.224$) are very close to each other, whereas the pore-filling model shows apparently larger values throughout. As already discussed, results from Archie's equation would be accurate as reference data, so the matrix-supporting model seems to be more applicable for use in studying the gas hydrate-bearing sediments in this area, implying that the hydrates are part of the sediment framework. Consequently, we conclude that the gas hydrates have reduced the original porosity and altered the elastic properties of the solid phase. Simultaneously, we have demonstrated that the established relationship between water-filled porosity and acoustic impedance is fairly applicable for estimating the spatial saturation.

Spatial saturation distribution of gas hydrate

The horizontal slice of inverted acoustic impedance at the BSR (Figure 6*a*) represents the maximum values extracted from a window with size of 10 ms above the horizon of the BSR. This slice depicts the overall spatial characteristics of gas hydrate occurrence. In Figure 6*a*, almost all of the relatively large values (> 3750 m/s × g/cm^3) are located in the south-east side

of the basin. The acoustic impedance distribution is directly related to the spatial distribution pattern of the BSR from the seismic data.

Using the empirical relationship between water-filled porosity and acoustic impedance obtained by the preceding method, we converted the acoustic impedance slice (Figure 6*a*) into an image of the spatial saturation of gas hydrates within the Kumano Basin (Figure 6*b*). The higher concentrations of gas hydrates occur primarily on the seaward side of the Kumano Basin, close to the outer ridge, and are oriented in a north-east–south-west direction (Figure 1*b*). The highest saturation is ~ 34%, with saturation values decreasing with increased distance from the seaward edge of the Kumano Basin. An anomalous saturation value occurs on the landward side of the centre of the study area, marked by point A in Figures 2*a* and 6*b*.

From Figure 2*a*, we note that the high hydrate concentration at point A is probably related to the splay fault activity in the accretionary wedge beneath the Kumano Forearc Basin (Tsuji et al., 2014*a*). A high amplitude (and low P-wave velocity) zone is observed above the ridge structure due to the ancient splay fault displacements (blue arrow in Figure 2*a*; Tsuji et al., 2015). Since this high amplitude zone is beneath the BSR, the anomaly cannot be identified in the horizontal slices in Figure 6. The reflection features can be interpreted as a high pore pressure or gas zone, and they indicate that some components of gas or fluid are derived through the splay fault in the accretionary wedge (Tsuji et al., 2015). On the other hand, the high hydrate saturation at point B in Figure 6*b* occupies the position of the mud volcano observed in Figure 2*b*, implying that this region experiences high pore pressure as well as an intensive methane supply. The association between high hydrate saturations with high pore pressures is consistent with the results of Toki et al. (2012). They suggested that the Kumano Basin sediments had a relatively high sedimentation rate, leading to organic matter burial without aerobic degradation on the surface of the seafloor. The organic matter, having been quickly buried, will subsequently degrade and generate gas, causing overpressure.

Discussion

The distribution patterns of gas hydrates are mainly controlled by the following factors: (1) methane supply, (2) temperature, (3) local pore pressure, and (4) lithology (Kvenvolden, 1993; Sloan and Koh, 2007; Waite et al., 2009). Here, we discuss migration and accumulation processes of gas hydrate from the results obtained in this study (Figure 7).

Lithology of the gas hydrate-bearing sediments

Because core samples were successfully recovered at Site C0002 from 200 mbsf to 502.8 mbsf, we are able to correlate the gas hydrate saturation depth profile with lithology. The dominant lithology in this depth interval is dark olive-grey silty claystone, and the minor lithologies include sandstone, sandy siltstone, silty claystone, calcareous claystone and fine ash (Strasser et al., 2014). The typical occurrence of sand in these cores takes the form of turbidite cycles that vary in sand thickness. The turbidite sand has an uneven distribution, being more abundant in the zones above 300 mbsf; nevertheless, the highest saturation of hydrate is close to the BSR (Figure 5). The sand occurrence from core samples demonstrated that there are significant thicknesses of cumulative sand and coarsest sand beds from 370 to 390 mbsf (Strasser et al., 2014), which corresponds to the depth of the highest saturation of gas hydrate in our estimation (Figure 5).

On the other hand, the low concentrations at 318.67 and 344.12 mbsf are related to beds with very low sand content (~6%) and sands that vanish at 302.5 mbsf to be replaced by a thick ash layer. The thicker and coarser sand beds have obviously facilitated the high concentration of the gas hydrates immediately above the BSR.

Migration path of the free gas

In the seismic section of inline 2529 (Figure 2*a*), the Kumano Basin sequence is cut by a series of normal faults. Many of these faults extend to the seafloor, and some of them cut the entire basin sequence into the underlying accretionary prism (Figure 6*c*; Moore et al., 2013). The genesis of these normal faults could be due to the extension from uplift at the seaward flank of the basin by the megasplay fault activities in the accretionary prism (Park et al., 2002; Gulick et al., 2010). In Figure 7*a*, we can observe acoustic impedance contrasts between the layers above and beneath the BSR. Admittedly, simple upward diffusion plays an important role in most cases regarding migration of free gas. Based on these observations and the local geologic setting in the basin, we postulate two new and different modes for the influx of free gas: (1) migration along the landward-dipping strata, and (2) migration from deep accretionary prism through the steeply dipping faults cutting through all of the basin sediments (Figure 7*b*).

Doan et al. (2011) found a gas enrichment interval and evidence of organisms at the bottom of borehole C0009A, and mentioned that these organisms probably play a role as a hydrocarbon source contributing to the observed gas distribution and the formation of gas hydrates in the Kumano Basin. Miyakawa et al. (2014) supported this hypothesis, but there is no direct evidence to prove the pathways as yet. Our results can support the interpretation of methane generation by organisms. As seen in Figure 7*a*, the acoustic impedance values of some strata (shown as green, indicated by black arrows in Figure 7*a*) at the landward side of the basin are lower than those (shown as red/yellow in Figure 7*a*) in surrounding areas. These layers are considered to be pathways for free gas migration as gas can reduce the P-wave velocity and bulk density of the sediments. When the free gas has migrated to point A (high hydrate saturation zone), the special configuration of faults (crossline No.7155 and 7350) would hinder further migration (Figure 2*a*), and the free gas could not be transported to the far seaward side of the Kumano Basin. Furthermore, as described above, an abnormally high amplitude (and low P-wave velocity) zone is located beneath the BSR just landward of point A (indicated by the blue arrow in Figure 7*a*). The reflection features could be interpreted as gas migrating through an ancient splay fault in the accretionary prism. Such gas also migrates to the point A in Figure 7*a*.

Because of the intense tectonic movements near the outer ridge, many local cracks or fractures that could be pathways for the upward migration of free gas are formed. Indeed, seismic anisotropy analysis has indicated that fractures are well developed due to oblique plate convergence at the margin close to the outer ridge (Tsuji et al., 2011*b*; 2014*b*). Meanwhile, pore pressure in the underlying accretionary prism is abnormally high on the seaward side of the Kumano Basin (Tsuji et al., 2014*a*), which means that free gas is forced to migrate upward along the faults or cracks. Generally, when the gas comes to the shallow sediments near the seafloor where the temperature and pressure are favourable,

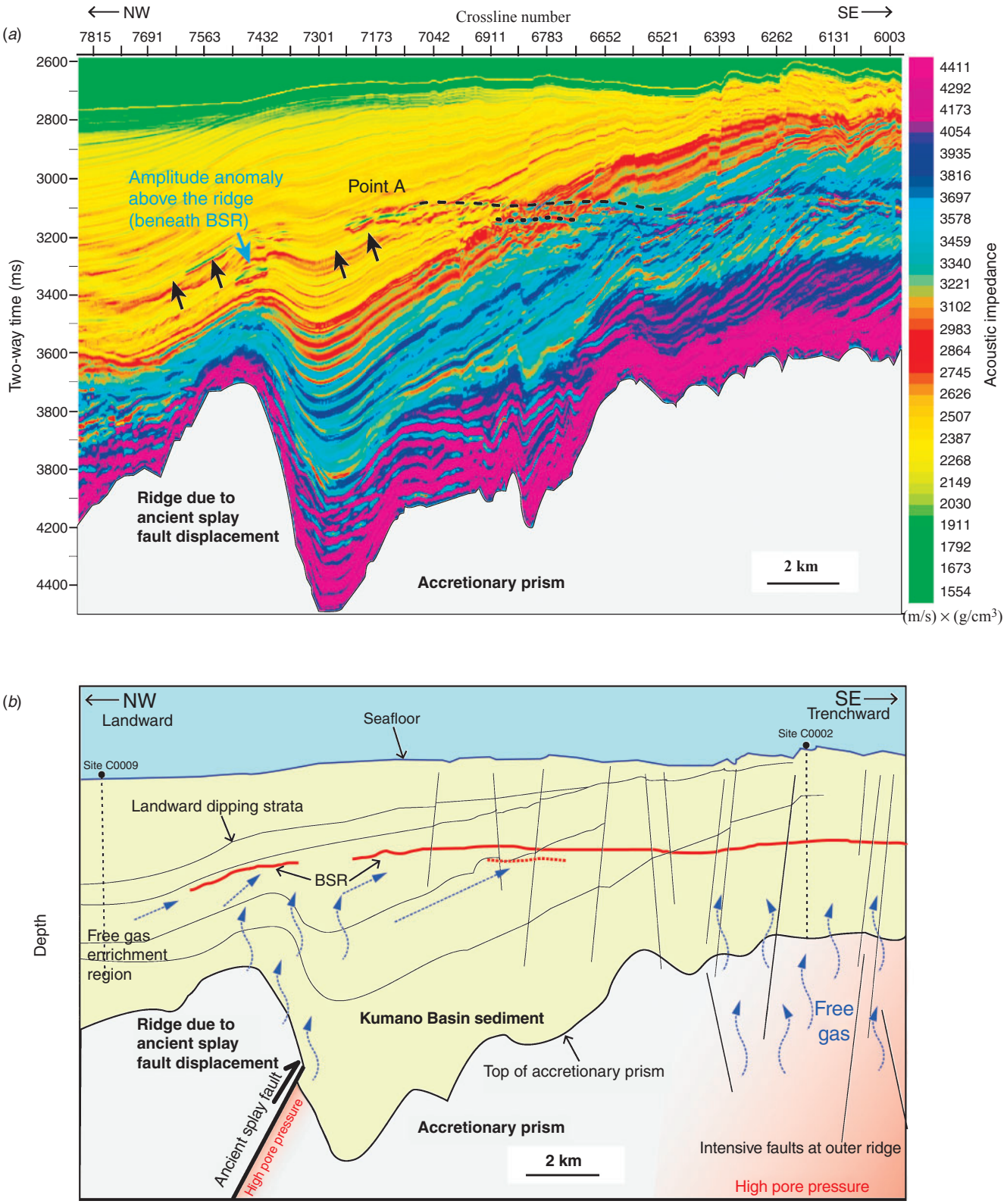

Fig. 7. (*a*) Estimated acoustic impedance from inline 2529 of the 3D seismic data. Black arrows represent the low acoustic impedance layers. The blue arrow indicates the amplitude anomaly (low velocity) above the ridge. (*b*) Schematic diagram of a representative model for the formation of the BSR (red line) and free gas migration (blue dashed arrows) in the Kumano Basin. The outer ridge is located near the south-east boundary of this profile. The red dashed line indicates the lower BSR.

gas hydrates are formed. Most of the areas of high concentration of gas hydrates in the south-east side of the Kumano Basin would be influenced by this mechanism.

In addition, a mud volcano (point B in Figure 6*b*) also controls the gas hydrate-bearing zone. In Figure 2*b*, we observe that the mud volcano appears to be based in the underlying accretionary wedge. The eruption enabled organic matter-bearing sediments (or free gas) in the underlying accretionary prism to move upward, and rapid gas accumulation in the shallow formation is conducive to the formation of gas hydrates. Pape et al. (2014) have discussed

the source of hydrocarbons related to mud volcano activity in the Kumano Basin, and have suggested that the most probable gas source for the mud volcanoes is derived from the old accreted sediments. Moreover, it has been proven by mud gas monitoring in borehole C0002F that thermogenic hydrocarbons prevail in the accretionary prism below 1700 mbsf (Pape et al., 2014). This interpretation is quite consistent with high-pressure conditions in the accretionary wedge close to the outer wedge (the red shaded zone in Figure 7*b*; Tsuji et al., 2014*a*).

Double BSR due to tectonic activity of the accretionary prism

Generally, the shape of the BSR on the seismic section is expected to be a single reflection with reverse polarity compared to the seafloor reflection, as can be seen between crosslines 6200 and 6510 in Figure 2*a*. However, from crossline 6672 to 7250, the BSR is blurred and thicker. We interpret this phenomenon to be the effect of the upward displacement of hydrates caused by tectonic uplift of the accretionary prism (Foucher et al., 2002). Tectonic movements occur frequently in the accretionary prism. Pressure and temperature conditions below the seafloor change accordingly, and gas hydrates would be destabilised as a result. The gas hydrates could decompose into free gas, which could then move upward along fractures and form new gas hydrates, resulting in the formation of a new active BSR, and the deeper BSR remains as a residual hydrate-related BSR. This process may lead to the co-existence of free gas and gas hydrates in the formation as has been identified by Miyakawa et al. (2014). In Figure 7*a*, we observe two interfaces (dashed and dotted lines in Figure 7*a*). Those interfaces cut across the strata at the depth of the BSR. The mechanism would be a reasonable explanation for this type of 'double BSR' within the Kumano Basin. On the other hand, we cannot discard other interpretations, such as a sea bottom warming effect, that may also generate 'double BSR' phenomenon (Foucher et al., 2002; Golmshtok and Soloviev, 2006).

These results demonstrate that tectonic activity of the accretionary prism (uplifting or subsidence) beneath the Kumano Forearc Basin could influence hydrate distribution as well as a migration process. Furthermore, we clarify that the fault or pore pressure distribution within the underlying accretionary prism is related to the hydrate saturation. Therefore, we conclude that when we characterise hydrate saturation or distribution in the forearc basin, we should consider the dynamics of the underlying accretionary prism. These implications are not solely related to the Kumano Forearc Basin in the Nankai Trough, but may also apply to forearc basins in other plate convergent margins.

Conclusion

The Kumano Forearc Basin is located on the landward side of the Nankai plate convergent margin in south-east Japan. The presence of gas hydrates in marine sediments of the Kumano Forearc Basin caused anomalies in the resistivity and P-wave velocity logs, and widespread BSRs on the seismic data. We have used these anomalies to predict the saturation of gas hydrates in the area. Based on the results, we have proposed mechanisms for the genesis of gas hydrate occurrence and a rock physics model for gas hydrates in this area, and offered the following conclusions:

(1) The occurrence of methane hydrate was successfully modelled by the matrix-supporting model. This result indicates that gas hydrates are attached to the surfaces of other minerals, and are not floating in the pore fluid.
(2) A spatial distribution of gas hydrates in the Kumano Forearc Basin was estimated; it showed that gas hydrates are highly concentrated near the outer ridge. The highest concentration of gas hydrates was ~34% in an area near the outer ridge.
(3) Reasonable explanations for the formation of gas hydrates are: (a) free gas that has migrated along the landward-dipping strata, and (b) free gas that has migrated upward through faults and cracks that cut through basin sediments.
(4) Overpressure zones and gas supply at the outer ridge and the ancient splay fault are responsible for hydrate generation. Therefore, the tectonic activities within the underlying accretionary prism significantly influence hydrate saturation and distribution in the Kumano Forearc Basin.

Acknowledgements

This paper benefited from constructive reviews and editorial handling of two anonymous reviewers and Editor K. Onishi. J. Jia visited Kyushu University for this study and gratefully acknowledges the financial support of the Ministry of Education, Culture, Sports, Science & Technology (MEXT), Japan. Hampson-Russell software for acoustic impedance inversion was provided by CGG. T. Tsuji gratefully acknowledges the support of JSPS through a Grant-in-Aid for Science Research B (no. 15H02988), Grant-in-Aid for Scientific Research on Innovative Areas (no. 15H01143), Grant-in-Aid for Scientific Research S (no. 15H05717) and Bilateral Joint Research Projects with MOSR. We further acknowledge JICA/JST through SATREPS project. We used borehole data provided by IODP, and seismic data provided by Japan Agency for Marine–Earth Science and Technology.

References

Archie, G. E., 1942, The electrical resistivity log as an aid in determining some reservoir characteristics: *Transactions of the American Institute of Mining, Metallurgical and Petroleum Engineers*, **146**, 54–62.

Ashi, J., Tokuyama, H., and Taira, A., 2002, Distribution of methane hydrate BSRs and its implication for the prism growth in the Nankai Trough: *Marine Geology*, **187**, 177–191. doi:10.1016/S0025-3227(02)00265-7

Baba, K., and Yamada, Y., 2004, BSRs and associated reflections as an indicator of gas hydrate and free gas accumulation: an example of accretionary prism and forearc basin system along the Nankai Trough, off central Japan: *Resource Geology*, **54**, 11–24. doi:10.1111/j.1751-3928.2004.tb00183.x

Boswell, R., 2013, Japan completes first offshore methane hydrate production test – methane successfully produced from deepwater hydrate layers: *Methane Hydrate Newsletter*, **13**, 1–2.

Collett, T. S., and Ladd, J., 2000, Detection of gas hydrate with downhole logs and assessment of gas hydrate concentrations (saturations) and gas volumes on the Blake Ridge with electrical resistivity data: *Proceedings of the Ocean Drilling Program: Scientific Results*, **164**, 179–191.

Collett, T. S., and Lee, M. W., 2012, Well log characterization of natural gas-hydrates: *Petrophysics*, **53**, 348–367.

Doan, M.L., Conin, M., Henry, P., Wiersberg, T., Boutt, D., Buchs, D., Saffer, D., McNeill, L.C., Cukur, D., and Lin, W., 2011, Quantification of free gas in the Kumano fore-arc basin detected from borehole physical properties: IODP NanTroSEIZE drilling Site C0009: *Geochemistry, Geophysics, Geosystems*, **12**, Q0AD06. doi:10.1029/2010GC003284

Dvorkin, J., and Nur, A., 1996, Elasticity of high-porosity sandstones: theory for two North Sea data sets: *Geophysics*, **61**, 1363–1370. doi:10.1190/1.1444059

Dvorkin, J., Prasad, M., Sakai, A., and Lavoie, D., 1999, Elasticity of marine sediments: rock physics modeling: *Geophysical Research Letters*, **26**, 1781–1784. doi:10.1029/1999GL900332

Ecker, C., Dvorkin, J., and Nur, A. M., 2000, Estimating the amount of gas hydrate and free gas from marine seismic data: *Geophysics*, **65**, 565–573. doi:10.1190/1.1444752

Expedition 314 Scientists, 2009*a*, Expedition 314 Site C0002, *in* M. Kinoshita, H. Tobin, J. Ashi, G. Kimura, S. Lallemant, E. J. Screaton, D. Curewitz, H. Masago, K. T. Moe, and the

Expedition 314/315/316 Scientists, eds, *Proceedings of the Integrated Ocean Drilling Program, 314/315/316*: Integrated Ocean Drilling Program Management International, Inc., 1–77.

Expedition 314 Scientists, 2009*b*, Expedition 314 methods, *in* M. Kinoshita, H. Tobin, J. Ashi, G. Kimura, S. Lallemant, E. J. Screaton, D. Curewitz, H. Masago, K. T. Moe, and the Expedition 314/315/316 Scientists, eds, *Proceedings of the Integrated Ocean Drilling Program, 314/315/316*: Integrated Ocean Drilling Program Management International, Inc., 1–33.

Expedition 315 Scientists, 2009, Expedition 315 Site C0002, *in* M. Kinoshita, H. Tobin, J. Ashi, G. Kimura, S. Lallemant, E. J. Screaton, D. Curewitz, H. Masago, K. T. Moe, and the Expedition 314/315/316 Scientists, eds, *Proceedings of the Integrated Ocean Drilling Program, 314/315/316*: Integrated Ocean Drilling Program Management International, Inc., 1–76.

Expedition 319 Scientists, 2010, Expedition 319 summary, *in* D. Saffer, L. McNeill, T. Byrne, E. Araki, S. Toczko, N. Eguchi, K. Takahashi, and the Expedition 319 Scientists, eds, *Proceedings of the Integrated Ocean Drilling Program 319*: Integrated Ocean Drilling Program Management International, Inc., 1–46.

Foucher, J. P., Nouze, H., and Henry, P., 2002, Observation and tentative interpretation of a double BSR on the Nankai Slope: *Marine Geology*, **187**, 161–175. doi:10.1016/S0025-3227(02)00264-5

Fujii, T., Saeki, T., Kobayashi, T., Inamori, T., Hayashi, M., Takano, O., Takayama, T., Kawasaki, T., Nagakubo, S., Nakamizu, M., and Yokoi, K., 2008, Resource assessment of methane hydrate in the eastern Nankai Trough, Japan: Offshore Technology Conference, 5–8 May, Houston, Texas, USA, 1–15.

Golmshtok, A. Y., and Soloviev, V. A., 2006, Some remarks on the thermal nature of the double BSR: *Marine Geology*, **229**, 187–198. doi:10.1016/j.margeo.2006.03.004

Gulick, S., Bangs, N., Moore, G., Ashi, J., Martin, K., Sawyer, D., Tobin, H., Kuramoto, S., and Taira, A., 2010, Rapid forearc basin uplift and megasplay fault development from 3D seismic images of Nankai Margin off Kii Peninsula, Japan.: *Earth and Planetary Science Letters*, **300**, 55–62. doi:10.1016/j.epsl.2010.09.034

Hamamoto, H., Yamano, M., Goto, S., Kinoshita, M., Fujino, K., and Wang, K., 2011, Heat flow distribution and thermal structure of the Nankai subduction zone off the Kii Peninsula: *Geochemistry, Geophysics, Geosystems*, **12**, Q0AD20. doi:10.1029/2011GC003623

He, L., Matsubayashi, O., and Lei, X., 2006, Methane hydrate accumulation model for the Central Nankai accretionary prism: *Marine Geology*, **227**, 201–214. doi:10.1016/j.margeo.2005.09.019

Helgerud, M. B., 2001, Wave speeds in gas hydrate and sediments containing gas hydrate: a laboratory and modeling study: D.Sc. thesis, Stanford University.

Helgerud, M. B., Dvorkin, J., Nur, A., Sakai, A., and Collett, T., 1999, Elastic-wave velocity in marine sediments with gas hydrates: effective medium modelling: *Geophysical Research Letters*, **26**, 2021–2024. doi:10.1029/1999GL900421

Inamori, T., and Hato, M., 2004, Detection of methane hydrate-bearing zones from seismic data: *Resource Geology*, **54**, 99–104. doi:10.1111/j.1751-3928.2004.tb00191.x

Kinoshita, M., Moore, G. F., and Kido, Y. N., 2011, Heat flow estimated from BSR and IODP borehole data: implication of recent uplift and erosion of the imbricate thrust zone in the Nankai Trough off Kumano: *Geochemistry, Geophysics, Geosystems*, **12**, Q0AD18. doi:10.1029/2011GC003609

Kvenvolden, K. A., 1993, Gas hydrates-geological perspective and global change: *Reviews of Geophysics*, **31**, 173–187. doi:10.1029/93RG00268

Lee, M. W., and Collett, T. S., 2001, Elastic properties of gas hydrate-bearing sediments: *Geophysics*, **66**, 763–771. doi:10.1190/1.1444966

Lu, S. M., and McMechan, G. A., 2002, Estimation of gas hydrate and free gas saturation, concentration, and distribution from seismic data: *Geophysics*, **67**, 582–593. doi:10.1190/1.1468619

Malinverno, A., Kastner, M., Torres, M. E., and Wortmann, U. G., 2008, Gas hydrate occurrence from pore water chlorinity and downhole logs in a transect across the northern Cascadia margin (Integrated Ocean Drilling Program Expedition 311): *Journal of Geophysical Research*, **113**, B08103. doi:10.1029/2008JB005702

Matsumoto, R., Tomaru, H., and Lu, H. L., 2004, Detection and evaluation of gas hydrates in the eastern Nankai Trough by integrated geochemical and geophysical methods: *Resource Geology*, **54**, 53–67. doi:10.1111/j.1751-3928.2004.tb00187.x

Mavko, G., Mukerji, T., and Dvorkin, J., 2009, *Rock physics handbook* (2nd edition): Cambridge University Press.

Milkov, A. V., 2000, Worldwide distribution of submarine mud volcanoes and associated gas hydrates: *Marine Geology*, **167**, 29–42. doi:10.1016/S0025-3227(00)00022-0

Miyakawa, A., Saito, S., Yamada, Y., Tomaru, H., Kinoshita, M., and Tsuji, T., 2014, Gas hydrate saturation at Site C0002, IODP Expeditions 314 and 315, in the Kumano Basin, Nankai Trough: *The Island Arc*, **23**, 142–156. doi:10.1111/iar.12064

Moore, G. F., Park, J. O., Bangs, N. L., Gulick, S. P., Tobin, H. J., Nakamura, Y., Sato, S., Tsuji, T., Yoro, T., Tanaka, H., Uraki, S., Kido, Y., Sanada, Y., Kuramoto, S., and Taira, A., 2009, Structural and seismic stratigraphic framework of the NantroSEIZE Stage 1 transect, *in* M. Kinoshita, H. Tobin, J. Ashi, G. Kimura, S. Lallemant, E. J. Screaton, D. Curewitz, H. Masago, K. T. Moe, and the Expedition 314/315/316 Scientists, eds, *Proceedings of the Integrated Ocean Drilling Program 314/315/316*: Integrated Ocean Drilling Program Management International, Inc., 1–46.

Moore, G. F., Boston, B. B., Sacks, A. F., and Saffer, D. M., 2013, Analysis of normal fault populations in the Kumano Forearc Basin, Nankai Trough, Japan: 1. Multiple orientations and generations of faults from 3D coherency mapping: *Geochemistry, Geophysics, Geosystems*, **114**, 1989–2002. doi:10.1002/ggge.20119

Nur, A., Mavko, G., Dvorkin, J., and Galmudi, D., 1998, Critical porosity: a key to relating physical properties to porosity in rocks: *The Leading Edge*, **17**, 357–362. doi:10.1190/1.1437977

Pape, T., Geprags, P., Hammerschmidt, S., Wintersteller, P., Wei, J., Fleischmann, T., Bohrmann, G., and Kopf, A. J., 2014, Hydrocarbon seepage and its sources at mud volcanoes of the Kumano forearc basin, Nankai Trough subduction zone: *Geochemistry, Geophysics, Geosystems*, **15**, 2180–2194. doi:10.1002/2013GC005057

Park, J. O., Tsuru, T., Kodaira, S., Cummins, P. R., and Kaneda, Y., 2002, Splay fault branching along the Nankai subduction zone: *Science*, **297**, 1157–1160. doi:10.1126/science.1074111

Pearson, C. F., Halleck, P. M., McGuire, P. L., Hermes, R., and Mathews, M., 1983, Natural gas hydrate: a review of in situ properties: *Journal of Physical Chemistry*, **87**, 4180–4185. doi:10.1021/j100244a041

Saffer, D., McNeill, L., Araki, E., Byrne, T., Eguchi, N., Toczko, S., Takahashi, K., and the Expedition 319 Scientists, 2009, NanTroSEIZE Stage 2: NanTroSEIZE riser/riserless observatory: Integrated Ocean Drilling Program Expedition 319 Preliminary Report, 1–83.

Saito, S., Miyakawa, A., Yamada, Y., and Kinoshita, M., 2010, Methane hydrate occurrence estimated from downhole logging at IODP Site C0002, Kumano basin: *Journal of the Japanese Association for Petroleum Technology*, **75**, 54–58. doi:10.3720/japt.75.54

Sloan, E.D. Jr, and Koh, C., 2007, *Clathrate hydrates of natural gases* (3rd edition): CRC Press.

Strasser, M., Dugan, B., Kanagawa, K., Moore, G. F., Toczko, S., Maeda, L., Kido, Y., Moe, K. T., Sanada, Y., Esteban, L., Fabbri, O., Geersen, J., Hammerschmidt, S., Hayashi, H., Heirman, K., Hupers, A., Jurado Rodriguez, M. J., Kameo, K., Kanamatsu, T., Kitajima, H., Masuda, H., Milliken, K., Mishra, R., Motoyama, I., Olcott, K., Oohashi, K., Pickering, K. T., Ramirez, S. G., Rashid, H., Sawyer, D., Schleicher, A., Shan, Y., Skarbek, R., Song, I., Takeshita, T., Toki, T., Tudge, J., Webb, S., Wilson, D. J., Wu, H.-Y., and Yamagushi, A., 2014, Site C0002, *in* M. Strasser, B. Dugan, K. Kanagawa, G. F. Moore, S. Toczko, L. Maeda, and the Expedition 338 Scientists, eds, *Proceedings of the Integrated Ocean Drilling Program, 338*: Integrated Ocean Drilling Program, 1–248.

Swisi, A. 2009, Post- and pre-stack attribute analysis and inversion of Blackfoot 3D seismic dataset: M.Sc. thesis, University of Saskatchewan.

Toki, T., Uehara, Y., Kinjo, K., Ijiri, A., Tsunogai, U., Tomaru, H., and Ashi, J., 2012, Methane production and accumulation in the Nankai accretionary prism: results from IODP Expeditions 315 and 316: *Geochemical Journal*, **46**, 89–106. doi:10.2343/geochemj.1.0155

Tsuji, Y., Namikawa, T., Fujii, T., Hayashi, M., Kitamura, R., Nakamizu, M., Ohbi, K., Saeki, T., Yamamoto, K., Inamori, T., Oikawa, N., Shimizu, S., Kawasaki, M., Nagakubo, S., Matsushima, J., Ochiai, K., and Okui, T., 2009, Methane-hydrate occurrence and distribution in the eastern

Nankai Trough, Japan: findings of the Tokai-oki to Kumano-nada methane-hydrate drilling program: *AAPG Memoir*, **89**, 228–246.

Tsuji, T., Hino, R., Sanada, Y., Yamamoto, K., Park, J.O., No, T., Araki, E., Bangs, N., Huene, R., Moore, G., and Kinoshita, M., 2011*a*, In situ stress state from walkaround VSP anisotropy in the Kumano Basin southeast of the Kii Peninsula, Japan: *Geochemistry, Geophysics, Geosystems*, **12**, Q0AD19. doi:10.1029/2011GC003583

Tsuji, T., Dvorkin, J., Mavko, G., Nakata, N., Matsuoka, T., Nakanishi, A., Kodaira, S., and Nishizawa, O., 2011*b*, Vp/Vs ratio and shear-wave splitting in the Nankai Trough seismogenic zone: insights into effective stress, pore pressure and sediment consolidation: *Geophysics*, **76**, WA71–WA82. doi:10.1190/1.3560018

Tsuji, T., Kamei, R., and Pratt, R. G., 2014*a*, Pore pressure distribution of a mega-splay fault system in the Nankai Trough subduction zone: insight into up-dip extent of the seismogenic zone: *Earth and Planetary Science Letters*, **396**, 165–178. doi:10.1016/j.epsl.2014.04.011

Tsuji, T., Ashi, J., and Ikeda, Y., 2014*b*, Strike-slip motion of a mega-splay fault system in the Nankai oblique subduction zone: *Earth, Planets, and Space*, **66**, 1–14. doi:10.1186/1880-5981-66-120

Tsuji, T., Ashi, J., Strasser, M., and Kimura, G., 2015, Identification of the static backstop and its influence on the evolution of the accretionary prism in the Nankai Trough: *Earth and Planetary Science Letters*, **431**, 15–25. doi:10.1016/j.epsl.2015.09.011

Uchida, T., Lu, H.L., and Tomaru, H., the MITI Nankai Trough shipboard scientists2004, Subsurface occurrence of natural gas hydrate in the Nankai Trough area: implication for gas hydrate concentration: *Resource Geology*, **54**, 35–44. doi:10.1111/j.1751-3928.2004.tb00185.x

Waite, W. F., Santamarina, J. C., Cortes, D. D., Dugan, B., Espinoza, D. N., Germaine, J., Jang, J., Jung, J. W., Kneafsey, T. J., Shin, H., Soga, K., Winters, W. J., and Yun, T. S., 2009, Physical properties of hydrate-bearing sediments: *Reviews of Geophysics*, **47**, RG4003. doi:10.1029/2008RG000279

Wang, X. J., Wu, S. G., Lee, M., Guo, Y. Q., Yang, S. X., and Liang, J. Q., 2011, Gas hydrate saturation from acoustic impedance and resistivity logs in the Shenhu area, South China Sea: *Marine and Petroleum Geology*, **28**, 1625–1633. doi:10.1016/j.marpetgeo.2011.07.002

Waseda, A., and Uchida, T., 2004, Origin and migration of methane in gas hydrate-bearing sediments in the Nankai Trough: *The Geochemical Society Special Publications*, **9**, 377–387. doi:10.1016/S1873-9881(04)80027-0